Cloud system resolving model simulations of tropical cloud systems observed during the Tropical Warm Pool-International Cloud Experiment

Kathrin Wapler*[1], Todd P. Lane[1], Peter T. May[2], Christian Jakob[3], Michael J. Manton[3], and Steven T. Siems[3]

[1]The University of Melbourne, Melbourne, Australia

[2]Centre for Australian Weather and Climate Research, Melbourne, Australia

[3]Monash University, Clayton, Australia

July 11, 2009

revised version

submitted as an article to *Monthly Weather Review*

*Now at: Deutscher Wetterdienst, Offenbach, Germany.

Corresponding author address: Kathrin Wapler, Deutscher Wetterdienst, GB Forschung und Entwicklung, Frankfurterstr. 135, 63067 Offenbach, Germany.

E-mail: kathrin.wapler@dwd.de

Abstract

Nested cloud system resolving model simulations of tropical convective clouds observed during the recent Tropical Warm Pool International Cloud Experiment (TWP-ICE) are conducted using the Weather Research and Forecasting (WRF) model. The WRF model is configured with a highest-resolving domain that uses 1.3 km grid spacing and is centered over Darwin, Australia. The performance of the model in simulating two different convective regimes observed during TWP-ICE is considered. The first regime is characteristic of the active monsoon, which features widespread cloud cover that is similar to maritime convection. The second regime is a monsoon break, which contains intense localized systems that are representative of diurnally forced continental convection. Many aspects of the model performance are considered, including their sensitivity to physical parameterizations and initialization time, and the spatial statistics of rainfall accumulations and the rain rate distribution. While the simulations highlight many challenges and difficulties in correctly modeling the convection in the two regimes, they show that provided the mesoscale environment is reproduced adequately by the model, the statistics of the simulated rainfall agrees reasonably well with the observations.

1. Introduction

The Tropical Warm Pool-International Cloud Experiment (TWP-ICE, May et al. 2008) took place in Darwin, Australia during January and February 2006. The experiment provided an extensive data set describing tropical cloud systems, their evolution and interaction with the large-scale environment. The experiment included a relatively dense network of ground-based observational systems including a polarimetric weather radar, cloud radar, wind profilers, radiation measurements, a lightning network and a balloon-borne sounding network. Additionally, five research aircraft were operated to measure cloud properties and the state of the atmosphere. The observational network was designed, in part, to facilitate thorough evaluation of cloud scale model simulations of the TWP-ICE period, and this paper explores the performance of nested cloud system resolving simulations of two periods of active convection during TWP-ICE.

The maritime continent and the northern parts of Australia are well known for regular convective activity in the summer months associated with the Australian monsoon (Drosdowsky, 1996). The convection in this region plays an important role in the energy budget and hydrological cycle of the tropics and thus strongly influences the global climate (Neale and Slingo 2003; DelGenio and Kovari 2002; Yang and Slingo 2001). For this reason, Darwin and surrounding regions (1) have been the focus of numerous field experiments examining tropical convection, e.g., the Australian Monsoon Experiment (AMEX, Holland et al. 1986; Gunn et al. 1989), the Island Thunderstorm Experiment (ITEX, Keenan et al. 1989), the Maritime Continental Thunderstorm Experiment (MCTEX, Keenan et al. 2000; Carbone et al. 2000) and the Darwin Area Wave Experiment (DAWEX, Hamilton et al. 2004; Pautet et al. 2005). In addition to the range of convective regimes experienced at Darwin, the neighboring Tiwi Islands experience an intense thunderstorm system, locally called *Hector*, that occurs regularly in the afternoon during

the October-November monsoon build-up and later in the season during monsoon break periods. Hector thunderstorms have been the focus of many of the aforementioned experiments and several numerical modeling studies (e.g., Golding 1993; Crook 2001; Lane and Reeder 2001).

As described by Drosdowsky (1996), the monsoon regime is characterized by westerly winds exceeding 10 m s^{-1} over a layer from the surface to 700 hPa. The active monsoon is associated with widespread convective activity, as a result of large-scale ascent, that appears similar in character to oceanic convection. The monsoon is interrupted by monsoon break periods (hereafter referred to as break periods), which contain storms more characteristic of continental convection. Convection in the break period is usually stronger, deeper and more isolated than during the active monsoon; it has a strong diurnal cycle, high lightning activity, and is often initiated by coastal circulation like sea-breezes (May and Ballinger 2007; Keenan and Carbone 1992). Within the two large scale regimes, 4 convective regimes may be defined (after May et al. 2008). These 4 regimes were sampled during the intense observing period of TWP-ICE. These were an active monsoon with widespread deep convection as well as a convectively suppressed monsoon period where convective clouds had limited vertical extent (tops below 8 km). Within the break period that followed the monsoon, there were some days of clear skies and a conventional break regime with deep electrically active convection. Examples of radar reflectivity measured for the active monsoon and the break period (Fig. 2) illustrate the fundamental differences between these flow regimes. The convection during the active monsoon is widespread, occurring over the land and ocean. In contrast, the break period convection occurs predominantly over land and is highly localized. Thus, these stark differences in cloud properties observed during TWP-ICE facilitate comparative studies of cloud processes in different convective regimes and provide the opportunity to examine the performance of numerical

models in these different regimes.

Cloud system resolving models (CSRMs) are valuable tools that provide complete and consistent datasets, allowing detailed studies of cloud processes and dynamics. While their past use has mostly been limited to research studies, CSRMs are an important component of modern numerical weather prediction (NWP) since advances in computer power are leading to reduced grid spacings and explicit representations of moist processes. Recent investigations have demonstrated the potential of cloud system resolving NWP to forecast severe convection (e.g., Kain et al. 2006; Done et al. 2004; Weisman et al. 2008), illustrating that the key improvements over predictions using parameterized convection are better forecasts of convective mode and more realistic patterns of clouds and precipitation. Furthermore, there is a growing trend in the use of CSRMs as dynamical downscaling tools for regional climate models. However, there remain significant uncertainties in the treatment of cloud microphysical processes and difficulties in the representation of the diurnal cycle of deep convection and precipitation. Thus, to improve CSRMs and maximize their representativeness of the physical environment, CSRMs require extensive and continued evaluation.

The central aim of this study is to examine the performance of the Weather Research and Forecasting (WRF) model (Skamarock et al. 2002) during the TWP-ICE period and to explore any regime-dependent aspects of this performance. In particular, this study focuses on the model's ability to reproduce the observed cloud structures and its performance in terms of precipitation, including area-averaged accumulated values and statistics of rain rates. Nested cloud system resolving simulations for the TWP-ICE period have been performed using the WRF model for two different periods, the first characteristic of the active monsoon and the second characteristic of the break period. Aspects of the model performance and its sensitivity to

model configurations and initialization time are examined, providing useful information about the use of nested models for downscaling applications and the representativeness of simulated convective structures for cloud process studies.

The paper is organized as follows. Section 2 presents the available observations and the meteorological conditions observed during TWP-ICE. Section 3 describes the model configurations and in section 4 the model simulations are compared to the observations. Finally, our summary and conclusions are presented in Section 5.

2. Observations and meteorological conditions

TWP-ICE provided a range of different observations, many of which have been used for the model evaluations described herein. Figure 1 illustrates the locations of the measurements in the TWP-ICE domain, demonstrating the geographic area of interest and the fact that the region is approximately equally divided between land and ocean. The TWP-ICE sounding, radar, flux and satellite observations were combined to form a model evaluation dataset, derived using the constrained variational objective analysis described in Zhang et al. (2001). The analysis includes measurements from radiosondes, precipitation radar, surface radiative and turbulence fluxes from the ocean and land stations, surface meteorological fields, cloud liquid water path and ECMWF model output to fill in gaps of missing data. The resultant dataset is representative of the conditions in the pentagon formed by the five radiosonde sites Mount Bundy, Point Stuart, Cape Don, Garden Point and Southern Surveyor (see Fig. 1) and in this study is used to describe the background conditions for model evaluation.

There are two sources of precipitation data. The first source is the 19 rain gauges distributed

around the experimental domain (Fig. 1), which all recorded precipitation accumulations at hourly intervals. The second source is from the 5.5 cm wavelength scanning polarimetric weather radar system located at Gunn Point (12.25°S, 131.04°E) near Darwin (Keenan et al. 1998). The rain rate was estimated from the radar using the algorithm described in Bringi et al. (2001, 2004) that uses a polarimetrically-tuned radar rainfall estimate involving estimation of the drop size distribution using radar measurements of the reflectivity factor at horizontal polarization, differential reflectivity, and specific differential phase. The radar-derived rain rate data has been mapped on a Cartesian grid with a horizontal resolution of 1 km.

As described in Section 1, the four regimes sampled during TWP-ICE were the active monsoon, a relative suppressed monsoon, some clear days and a break period. While there are various definitions of monsoon conditions (e.g., Drosdowsky 1996), in Darwin the principal feature of active monsoon periods is the presence of westerly winds between 850 and 700 hPa. Here a simple definition of westerlies at 700 hPa in a 4 day smoothed wind time series is used to identify regimes. In addition to this definition, the four distinct regimes are clearly identified by the time series of the mean accumulated precipitation during TWP-ICE (Fig. 3). During the active monsoon period a variety of convective organization occurred, including isolated storms as well as convective lines. This period showed the highest cloud occurrence of the TWP-ICE experiment, and the area-averaged rain rate during the active monsoon period was around 17 mm/day. Towards the end of this period a large mesoscale convective system (MCS) developed, which produced an area-averaged accumulated rainfall of more than 70 mm/day. In contrast, the break period was characterized by intense afternoon thunderstorms as well as several squall lines passing through the TWP-ICE domain during the evening and early morning. Due to the relatively transient and localized nature of the convection during the break period,

the area-averaged rain rate was only 8 mm/day. See May et al. (2008) for a more detailed description of the meteorological situation during TWP-ICE.

3. Model configuration

The Weather Research and Forecasting (WRF) model is a compressible nonhydrostatic finite difference model designed for both research and operational applications (see Skamarock et al. 2002, for details). The WRF model allows flexible domain configurations, including nested grids that can focus on regions of interest with higher resolution domains. The model has numerous physics options, including a number of boundary layer, surface, radiative transfer, cloud microphysics, and cumulus parameterization schemes. The WRF model has been used during a number of recent field experiments and coordinated forecasting programs (e.g., Done et al. 2004; Kain et al. 2006; Weisman et al. 2008) and will be used for all simulations reported herein.

Simulations for two different periods have been performed using version 2.2 of the Advanced Research WRF (WRF-ARW). The WRF simulations were performed with four one-way nested domains with horizontal grid spacings of 34, 11.333, 3.778, and 1.259 km, each with 64 vertical levels; see Fig. 4 and Table 1 for the horizontal locations and geometries of these domains. The innermost (cloud system resolving) domain, which is the focus of most of our analysis, is centered over the Gunn Point radar near Darwin and covers an area of 307 km $\times$ 307 km. The WRF model was initialized using the NCEP $1^o \times 1^o$ global operational analysis, which also provided boundary conditions to the outermost domain at 6-hourly intervals. The number of the nested domains and their resolution was chosen to have the recommended

ratio of 3 between the resolution of the input data, the outer domain and the nests down to a grid resolution of the order of 1 km. Furthermore, the use of one-way nesting facilitates more straightforward interpretation of the larger-scale controls on the modeled convection. The model was configured using the long-wave Rapid Radiative Transfer Model (RRTM Mlawer et al. 1997), the shortwave MM5 (Dudhia 1989) radiation, thermal diffusion surface scheme, and the Purdue Lin microphysical scheme (Chen and Sun 2002). Unless otherwise stated, the simulations use the Mellor-Yamada-Janjic (MYJ) boundary layer scheme (Janjic 2002), and the Kain-Fritsch cumulus parameterization scheme (Kain and Fritsch 1990, 1993; Kain 2004) in the two outermost domains. Two separate simulation periods are considered; the first period, 1200 UTC 20 January 2006 to 1800 UTC 24 January 2006 is representative of the active monsoon; and the second period, 1200 UTC 5 February 2006 to 1800 UTC 9 February 2006 is representative of the break period. Figure 5 shows an example of model-derived radar reflectivities for the two simulated periods; see Table 2 for a summary of all simulations that will be described in this study.

The configuration of WRF and its nesting within the NCEP analyses is designed primarily to examine the mesoscale response to large-scale forcing as well as the response from local forcings derived from coastal circulations. However, the use of analyses as boundary conditions removes any true predictive interpretation of these results, but allows controlled experiments to be undertaken and provides WRF with the best opportunity to agree with the observations. Nonetheless, as shown in Fig. 4, the outermost boundary is a significant distance from the region of interest and therefore the model solution in the vicinity of Darwin is only weakly constrained by the NCEP analyses. In addition to interpretation of model performance, this configuration is also directly relevant to the assessment of similar downscaling approaches, either for NWP

or climate applications. To evaluate model solutions, the WRF results will be compared to the TWP-ICE observations, including the model evaluation dataset. The additional observations made during TWP-ICE, e.g., the 3-hourly radiosondes from five different sites surrounding Darwin, were not included in the NCEP analysis and do not compromise the comparisons to the WRF simulations because they are an independent dataset.

4. Comparison of model results and observations

a. Overall model performance

The active monsoon and break periods are characterized by different environmental conditions, as illustrated by the temporal evolution of the horizontal velocity, vertical velocity and relative humidity from the TWP-ICE evaluation dataset (Fig. 6). During the active monsoon period westerly winds were present between 700 and 850 hPa, followed by an easterly shift of the low-level winds on day 23, which preceded the large mesoscale convective system (MCS). The wind had a southerly component, except during the occurrence of the MCS. The vertical velocity is predominantly upwards throughout the period, with a strong maximum in the early morning of day 24, associated with the MCS, and a secondary nocturnal maximum in the early morning of day 23 (Fig. 6c). There was limited variability in relative humidity throughout the active monsoon period, with high values throughout the troposphere (Fig. 6d). The wind in the break period was predominantly easterly with a shallow westerly flow in the boundary layer; the meridional component of the wind showed no consistent direction throughout the period. In contrast to the active monsoon period, the break was accompanied by a very dry middle and upper troposphere, especially on day 39 (Fig. 6h). The vertical velocity shows mean descent

in the mornings followed by a coherent signal of stronger mean ascent in the afternoons. This ascent is of similar strength on days 37, 38, and 40, but is weaker and less coherent on the afternoon of day 39 (Fig. 6g).

Figure 7 shows the simulated mean horizontal velocity, vertical velocity, and relative humidity from the reference simulations MONSOON-0 and BREAK-0 (see Table 2), calculated over the area of the inner domain (see Fig. 4). Both simulations show good representations of the observed winds (Fig. 6), reproducing the important differences: lower-tropospheric westerlies during the active monsoon and easterlies during the break. The strength of the shift from low-level westerly to easterly winds during the passage of the MCS in MONSOON-0 is slightly underestimated in the simulations. However, in general, the simulated horizontal wind components are in good agreement with the observations; of particular importance here is the agreement in the wind direction, which helps define the convective regime. In addition, the overall characteristics of the humidity distribution in the two periods is correctly represented by the model. The largest difference between observed and simulated humidity is visible during the break in the upper troposphere, which is too humid in the simulation.

The largest difference between the model simulations and observations is found in the vertical velocity field. While the simulated vertical velocity during the active monsoon period shows many similarities and is mostly the same sign as observed, the upward motion in MONSOON-0 is generally smaller than depicted in Fig. 6c. Furthermore the overall timing of the ascent within the MCS is reproduced well, except the secondary maxima in upward velocity at the onset of day 23 is not present in the model. On the other hand, the break simulations, BREAK-0, shows vertical velocities of similar magnitude to those observed, yet the vertical velocity is out of phase with the observations. The simulated maxima in upward motion occur during the

middle of the night, with subsidence during the afternoon (Fig. 7g), i.e., there is modeled subsidence during the period of maximum observed convective activity; these errors are particularly evident on day 1 and 2 of the BREAK-0 simulation. Of course, the upward component of the vertical velocity is comprised of a combination of the large-scale forcing and the upward mass flux derived from convective cores.

The time series of area averaged rain rates during the two different periods are shown in Fig. 8, along with the equivalent radar-derived estimates. Both of these averages are constructed over the circular area of 150 km radius that corresponds to the horizontal range of the radar. During the active monsoon the observed and simulated area averaged rain rates are higher than during the break period (note different scales in Fig. 8), due to the more localized nature of the break convection. During the active monsoon daily precipitation totals are well simulated by the WRF model on all days, reproducing many of the significant rainfall events, and with a four-day rainfall accumulation of 105 mm that compares very well to observations (113 mm). However, the simulation fails to reproduce much of the short-scale temporal variability in the observed time series and does not produce the nocturnal precipitation event between days 2 and 3, likely due to the incorrect simulation of the vertical motion at this time. Despite of these differences, a major success of the simulation is evident on day 4, where WRF reproduces the sizable precipitation totals associated with the large MCS. The simulated precipitation on this day, however, begins about two hours too late and lasts about two hours longer in total duration. This event will be examined in more detail in Section 4c.

The break period simulation also shows good agreement with the intensity of the observed rainfall events, and the simulated four-day accumulations of 29 mm are similar to the observed accumulations (21 mm). During this period, however, the details of the observed precipitation

are poorly represented by the simulation. The model simulates strong nighttime precipitation in the first two nights and only very little precipitation on day 4. In contrast, the observations show that these days were clearly dominated by afternoon precipitation. The poor representation of the diurnal cycle of precipitation is a consequence of the incorrectly simulated diurnal cycle of vertical velocity seen above; these processes will be examined in more detail in the next section.

As a test of the sensitivity of the model results to variations in the boundary layer parameterization, simulations were also performed using the Yonsei University (YSU) scheme (Hong and Dudhia 2003) instead of the Mellor-Yamada-Janjic (MYJ) scheme. The results (not shown) indicate a much better model performance with the MYJ scheme (see Wapler et al. (2008) for details). The YSU scheme over-represents the strength of the diurnal cycle of humidity, resulting in the daytime boundary layer being too dry. Comparisons with measurements from surface flux stations reveal that the sensible heat flux is strongly overestimated and the latent heat flux underestimated in the simulation with the YSU scheme. This results in a overestimation of the Bowen ratio by a factor of more than 2 compared to observations. The simulations with the MYJ scheme have a Bowen ratio that is only slightly higher than observed. For these reasons, the MYJ scheme was used for all simulations presented herein. Similar sensitivities have also been identified over the continental United States (e.g., Weisman et al. (2008)).

Additional simulations were performed using two-way nesting instead of one-way nesting. These simulations show only marginal differences and no improvement over the BREAK-0 simulation.

b. Sensitivity to the application of cumulus parameterization

The previous section highlighted the relatively good performance of the WRF model in reproducing the large-scale environmental conditions and precipitation accumulations during the active monsoon period. However, during the break period there were important differences in the simulated diurnal cycle of the convection, associated with large-scale mean descent during the afternoon. These simulations all used parameterizations of cumulus convection in the two outermost (non cloud system resolving) domains; these domains ultimately control the background flow conditions, including mean ascent and descent, for the two interior domains. It is well known that models with parameterized convection have difficulty simulating the diurnal cycle of convection in the tropics (e.g., Wang et al. (2007)), which may be the cause of the issues in the break simulation. Furthermore, as shown by Warner and Hsu (2000), high resolution CSRMs nested within coarser resolution domains (with parameterized convection) can experience a detrimental influence from the effects of the cumulus parameterization. While it may seem physically inappropriate, Warner and Hsu (2000) showed that nested CSRM performance can be improved if cumulus parameterizations are not used on the coarser resolution domains. With this in mind, the WRF simulations are re-run without using cumulus parameterization for any of the domains; these simulations are denoted MONSOON-1 and BREAK-1 (see Table 2). The horizontal average of the simulated fields from domain 4 are shown in Fig. 9 and the time series of precipitation are shown in Fig. 10.

During the active monsoon period the mean horizontal velocity is similar in the MONSOON-0 and MONSOON-1 simulations in the first 3 days. However, towards the end of the MONSOON-1 simulation there are northeasterly winds in the middle troposphere (Fig. 9a-b) compared to north-westerlies in MONSOON-0 (Fig. 7a-b) and the observations (Fig. 6a-b). On day 23 the

MONSOON-1 simulation shows mean ascent followed by descent during night and fails to simulate the convection in the night and morning of day 23 (Fig. 9c) and does not produce mean ascent during the passage of the MCS. These deficiencies are clearly evident in the time series of simulated precipitation (Fig. 10a), and the lower values of humidity (Fig. 9d) during the period of the observed MCS. Time-height cross-sections of the differences in the mean profiles of the MONSOON-0 and MONSOON-1 simulations reveal the changes introduced due to the presence of cumulus parameterization on the outer domains (Fig. 11a-c). The simulation with cumulus parameterization possesses weaker vertical ascent in the first three days, especially during the daytime, along with dryer and warmer conditions below 4 km and weaker warming and moistening further aloft. From the afternoon of day 3 until the end of the simulation the MONSOON-0 simulation produces the large MCS, which propagates into Domain 4 from the coarser resolution domains; without cumulus parameterization the MCS does not form. In summary, it is clear that the model performance is superior in MONSOON-0, when the cumulus parameterization is active on Domains 1 and 2.

Similar to the simulations of the active monsoon, the BREAK-1 and BREAK-0 simulations show very similar distributions of horizontal wind. However, the BREAK-1 simulation (without cumulus parameterization) leads to considerable improvements in the simulated vertical velocity (Fig. 9g) and precipitation (Fig. 10b) in comparison to the BREAK-0 simulation. In particular, Fig. 10b shows excellent agreement between simulated and measured rain rates for the break period on day 1, 2 and 4, capturing the timing and intensity of all major precipitation events on these days. This agreement in precipitation is consistent with the vertical velocity (Fig. 9g); the simulated mean vertical velocity shows ascent during the afternoon which is in phase with the observations. The largest discrepancy between the BREAK-1 simulation and the

observations occurs on Day 3, where simulated precipitation is initiated in the early morning on a day when very little precipitation was actually observed. The reasons for this erroneous convective initiation and its sensitivity to model initialization time will be described in Section 4c.

The afternoon descent evident in the BREAK-0 simulation (Fig. 7g) is remediated in the BREAK-1 simulation (Fig. 9g), which features weak daytime ascent in the lower troposphere, beginning around midday on Day 1 and 2. The differences between the BREAK-1 and BREAK-0 simulated potential temperature and mixing ratio (Fig. 11) are consistent with this difference in vertical motion, with distinct features identifying reduced lower tropospheric moisture and warming in the afternoons of the BREAK-0 simulation. It seems likely that the simulated daytime descent in the BREAK-0 simulation is suppressing the observed daytime convective development, with the largest difference between the BREAK-0 and BREAK-1 simulation occurring at around 3 km altitude. This daytime descent over Darwin is not present in the NCEP analysis data (not shown), implying that the descent originates from the coarser resolution WRF domains. To investigate the origin of this large scale descent, the 3 km vertical velocity from Domain 1 is examined for both the BREAK-0 and BREAK-1 simulations (Fig. 12) at 1330 LT on Day 1 of the break simulation (the time at which the largest differences in vertical velocity are first evident). Fig. 12 shows a distinctly different vertical velocity distribution between the two cases. In the BREAK-0 simulation the vertical velocity highlights large contiguous areas of ascent over northeast and northwest Australia, associated with parameterized convection over those regions. Conservation of mass requires compensating subsidence to occur and because the ascent in BREAK-0 occurs over such large areas the descent is relatively strong in regions where convection is not active, such as over the oceans and the Darwin region. On the other

hand, the BREAK-1 simulation produces more intense and highly localized and poorly resolved storms over northwest and northeast Australia, yet because of the localized (and unphysical) nature of these storms the compensating subsidence is local and does not have a remote influence on the Darwin region. Satellite observations of the region on this day (not shown) illustrate that convection is indeed most active over northwest and northeast Australia, as simulated by BREAK-0 and BREAK-1; the area of ascent associated with the convection is likely somewhere between that simulated by BREAK-0 and BREAK-1, which would presumably lead to limited influence by large-scale compensating subsidence on the Darwin region.

One consequence of the large-scale descent evident in the BREAK-0 simulation is illustrated in Fig. 13, which shows the level of free convection (LFC) and the boundary layer depth for both BREAK-0 and BREAK-1. In both simulations the boundary layer grows to a similar depth. In the BREAK-1 simulation the LFC is low enough such that it is within the mixed layer during the afternoon, allowing deep convection to develop through simple boundary layer ascent. However, the descent during the BREAK-0 simulation increases the height of the LFC slightly so that it is above the boundary layer, which prohibits deep convective initiation (by boundary layer ascent) in the afternoon. As illustrated by the similar boundary layer depths, and the difference fields (Fig. 11) there are only minor differences in surface properties on Day 1 for the BREAK-1 and BREAK-0 simulations, although these differences become larger as the simulation continues. Thus the differences between the levels of free convection that arise on Day 1 are mostly due to changes in thermodynamics near the boundary layer top (associated with descent).

These results, highlighting the detrimental influence of circulations generated on coarser resolution domains, are consistent with the findings of Warner and Hsu (2000). To investigate

whether this result was a unique response to the Kain-Fritsch parameterization, additional simulations were performed for the break period using the Betts-Miller-Janjic (Betts and Miller 1993; Janjić 1994) and the Grell-Devenyi (Grell and Dévényi 2002) cumulus parameterization scheme instead of the Kain-Fritsch scheme. These additional simulations (not shown) did not show any significant improvement over the BREAK-0 simulation, and none were as successful as BREAK-1 in reproducing the diurnal cycle of precipitation.

From the discussion above it is evident that the choice of model configuration to obtain the best Domain 4 performance is regime dependent, which is certainly not a desirable result. Furthermore, while the BREAK-1 simulation produces good performance on Domain 4, its simulated convection on the outer domains is unphysical. Nonetheless, it is still useful to examine the features within the high-resolution domain for those simulations that provide the best model performance. Therefore, the remainder of this paper will focus on results from model configurations with cumulus parameterization in the outer domains for the active monsoon (MONSOON-0) and without cumulus parameterization for the break period (BREAK-1).

c. Sensitivity to initialization time

While the BREAK-1 and MONSOON-0 simulations show a good representation of the four-day precipitation time series and accumulations, there are notable errors. For example, Day 3 of Break-1 shows erroneous convective initiation and MONSOON-0 does not reproduce the precipitation event at midnight between Day 2 and 3. While the WRF simulations are all constrained by the NCEP analysis boundary conditions, model errors and biases can accumulate reducing the quality of multi-day simulations as well as contributions from the growth of initial condition errors. This, of course, is a well-known feature of numerical weather prediction,

and as shown by Lo et al. (2008) can reduce the quality of dynamical downscaling methods. In this section we briefly explore the sensitivity of the WRF simulations to initialization time. The model runs MONSOON-2, MONSOON-3 and MONSOON-4 are initialized 24 hours apart (table 2), thus each day of the 4-day period is the first day in one of the new simulations. The simulations BREAK-2, BREAK-3 and BREAK-4 are initialized analogously (table 2). These sets of simulations are configured the same way as MONSOON-0 and BREAK-1, respectively.

While differing in details, MONSOON-2 performs similarly to MONSOON-0 and does not simulate the nighttime precipitation between Days 2 and 3 (Fig. 14). On monsoon day 3 the model run MONSOON-3 incorrectly simulates morning precipitation; this simulation is initiated in the middle of the Day 2-3 precipitation event and is likely unduly influenced by model spin-up during this period. In contrast, all of the simulations produce the day 4 MCS, however the onset of precipitation differs by about four hours between the cases, along with differences in the location and intensity. The beginning of precipitation of the MCS on the evening of day 3 is correctly simulated in the MONSOON-2 run, the precipitation in the MONSOON-0 run starts approximately two hours too late, in the MONSOON-3 run two hours to early. The maximum area-averaged rain rate is accurately simulated in all runs, but the longevity of the system and the total amount of precipitation is overestimated in the simulations MONSOON-2 and MONSOON-3. However, as shown in Fig. 15, the location of the maximum precipitation is more accurately simulated in MONSOON-2 and MONSOON-3 than MONSOON-0. The initialization time of the MONSOON-4 run coincides with the beginning of the MCS precipitation. The model immediately produces precipitation and simulates the correct total amount of precipitation, however the location of the MCS is not simulated as well as in runs MONSOON-2 and MONSOON-3 (not shown). These simulations highlight that the Day 4 MCS is a robust feature

of all of the active monsoon simulations, suggesting that the forcing for this phenomenon is present in the NCEP analysis.

The BREAK-2 and BREAK-3 simulations show an improvement in the simulation of day 3 (Fig. 16), both simulations correctly simulate no precipitation in the early morning. Closer examination of the early morning BREAK-1 precipitation fields suggest that the convection initiated in the model arises from an intense land-breeze circulation in the model. This circulation initiated convection off shore, having negative influences on the simulated flow in the Darwin region for the remainder of the day. More detailed analysis of this and observed cases of land breeze convective initiation will be described in a later study. On day 4 the morning precipitation is only simulated by BREAK-1, however BREAK-2, BREAK-3 and BREAK-4 show an improvement in simulating the timing of the onset of afternoon convection. Although the amount of precipitation is underestimated in model runs BREAK-3 and BREAK-4, they correctly simulate the onset of precipitation in the late evening of day 4.

As demonstrated above, model runs with different initialization times show significant differences in the timing, occurrence, location, and intensity of precipitation. Even though the simulations initialized closer to an event show some improvements, not all aspects of the precipitation event are better simulated. Among other things, the above results highlight the potential utility of ensemble simulations of these systems.

d. Evaluation of simulated cloud structure and precipitation statistics

In this section the results from the MONSOON-0 and BREAK-1 simulations are analyzed in more detail to determine how the physical characteristics and statistics of the cloud and precipitation distributions compare to those observed.

As illustrated in the simulation results, the cloud systems occurring during the active monsoon period and the break periods possess substantial differences between their extent, vertical distribution, and rainfall statistics. These differences are highlighted in Fig. 17, which shows observed cloud frequency and simulated cloud fraction. The simulated cloud fractions are calculated as the proportion of cloudy grid points at each altitude over the areal range of the radar. A model grid point pixel is considered 'cloudy' if the derived reflectivity (after Stoelinga 2005) exceeds -30 dBZ. These simulated cloud fractions are compared to cloud frequencies observed by the upward pointing 35 GHz cloud radar at the ARM site in Darwin. The cloud frequencies are calculated from counting the fraction of time that the radar detects a cloud. The sensitivity of the radar was approximatedly -28 dBZ at 15 km. Even for a perfect simulation of cloud distribution, the cloud fraction from the model domain shouldn't necessarily be the same as that derived from a single point observation within the domain. Furthermore, one vertically pointing radar isn't always representative of the surrounding area. Especially if the domain is highly heterogenous in its amount and type of precipitation. Nevertheless, these observed frequencies provide a source of model validation (Jakob et al. 2004). Figure 17 shows that the active monsoon featured extensive cloud cover throughout the troposphere whereas the break period shows lower cloud fractions with two maxima, one in the lower and one in the upper troposphere. The second maximum results from cirrus formed by the outflow of deep convection. The simulated cloud fraction shows good agreement with the observations, representing the key features of the cloud fraction distribution. There are, however, notable differences. For example, during the active monsoon the simulation show a larger depth of the convection and a larger coverage in the upper-troposphere. This may be due to difficulties of detecting high level clouds with radar in the presence of a deep cloud layer. The break simulation under estimates the coverage

of ice in the upper-levels, potentially highlighting inadequancies in the microphysics scheme or simply reflecting limitations in these comparisons. Also, one significant difference between the modeled and observed convection in the active monsoon is that low clouds are under represented by the model. Such clouds are possibly small cumulus that would be poorly resolved by the 1.3km resolution domain.

As shown in typical examples of observed reflectivity (Fig. 2) the convection during the active monsoon was very wide-spread with a maritime character, in contrast to the scattered, localized continental convection during the break period. In general, during the break period individual convective cells attained higher values of reflectivity than in the active monsoon. These differing patterns are also present in the simulations (Fig. 5). The different characteristics of precipitation during these two periods can be seen in time series of mean rain rates separated between land and ocean (Fig. 18). During the monsoon the precipitation occurs more evenly spread over land and ocean. In contrast, a large difference between precipitation over land and ocean is visible during the break period. The diurnal cycle over land is clearly dominated by afternoon precipitation whereas offshore precipitation mainly occurs in the early morning. These features are mostly well represented by the the simulations in both regimes.

In addition to accumulated values, the statistics of rainrates are also analyzed as a more stringent measure of model performance. Figure 19 shows observed and simulated areas that are affected by at least 10 mm/h. With the exception of the incorrectly simulated precipitation event during night 2-3 of the monsoon and day 3 of the break period, Fig. 19 demonstrates that these strongest rain rates are well represented by the model.

Further insight in rain statistics of the two periods is gained by examining histograms of spatial occurrence of accumulated precipitation values and rain rates (Fig. 20) for the model,

the rain gauge network (only for rain rates), and the radar observations. In both regimes, the largest differences arise between the coverage of simulated and radar-observed low rain rates, with the simulated coverage of low rain rates (< 3 mm/hr) being significantly larger. Sampling and quality control issues result in the radar not detecting the smallest rain rates, explaining at least some of the differences. Furthermore, the rain gauges and the model show good agreement in the active monsoon at these small rain rates, further suggesting that these differences are likely a radar sampling issue. However, the model and gauges do not show good agreement at these low rain rates during the break period; yet, the number of gauges may be simply too small to provide a robust representation of the highly localized break convection. Furthermore, the rain gauges were only present over the land and thus not absolute representative of the entire domain. The spatial statistics of the 4-day accumulated rainfall (Fig. 20c-d) illustrates that the model simulations reproduce the observed distribution very well, distinguishing between the widespread rainfall of the active monsoon and the localized convection of the break. These statistical measures provide a stringent test of the model performance that are not unduly affected by the randomness of deep convection.

These comparisons demonstrate that the WRF model simulations effectively delineate the important differences between the active monsoon convection and the break convection. While these simulations suffer errors in the timing and occurrence of some convective events, the statistical evaluations have demonstrated that the precipitation rates and accumulations are realistic. These results suggest that provided the model can produce a good representation of the background mesoscale flow, the statistics of the rainfall can be realistically reproduced at the cloud system resolving scale. However, to decrease the problem of timing and location error mesoscale ensemble prediction techniques are valuable for specific weather prediction.

5. Summary and Conclusions

Cloud system resolving model simulations of tropical cloud systems observed during TWP-ICE have been performed using the Weather Research and Forecasting (WRF) model. Comparisons with available observations have been presented that enable assessment of the model's performance in simulating tropical convection, and its regime dependence. These results have important implications for assessing the use of cloud system resolving models for cloud process studies and dynamical downscaling approaches.

Two different periods characteristic of the active monsoon and the break period have been simulated with a multi-nested model set-up. These simulations showed that it was necessary to use judicious choices of model settings to achieve the best simulation within the highest resolution domain. In particular, during the break period, the highest resolution domain was unduly affected by large-scale descent that originated from parameterized convection remote from our region of interest. The result of this descent was a poorly produced diurnal cycle that was remediated by not using a convective parameterization on the coarser resolution domain; an approach that is far from ideal. This result agrees with previous work (e.g., Warner and Hsu (2000)) and suggests one difficulty in the nested modelling approach.

A series of simulations were also conducted to determine the sensitivity of the simulated precipitation to model initialization time. These results suggested that in some scenarios a shorter model lead-time was beneficial in producing better simulations of some precipitation events, but this was not necessarily true for all cases. These tests highlighted the large sensitivity of the simulated convection to initiation time, suggesting that an ensemble approach is likely most desirable, even for downscaling applications.

In addition to producing good representations of the mean precipitation accumulations over

our area of interest, an important result of this study concerns the evaluation of the statistics of the precipitation rate and accumulations. The model simulations were shown to reproduce the spatial statistics of precipitation accumulations and rainrates in the two regimes. This result suggested that at the cloud system resolving scale the statistics of the rainfall distribution are realistic. The agreement was true for both regimes suggesting that realistic rainfall distributions can be reproduced provided the mesoscale flow that characterizes that regime is simulated by the model.

These results have examined a few realizations of the WRF model during the TWP-ICE period highlighting strengths and deficiencies in the model's performance. Such evaluations provide the basis for further studies into cloud processes in the tropics using WRF that can be used for model development activities from the cloud through to the climate model scales.

Acknowledgments

This work is supported by the Australian Research Council Discovery Projects funding scheme (DP0770381). Computing facilities were provided by the Victorian Partnership for Advanced Computing. We would like to thank Michael Whimpey for providing the radar data, and Timothy Hume for the rain gauge data. Thankyou to Simon Caine for his assistance with the model configuration, and to Rit Carbone and one anonymous reviewer for their useful comments that helped improve the manuscript.

References

Betts, A. K. and M. J. Miller, 1993: The Betts-Miller scheme. *The representation of cumulus convection in numerical models*, Amer. Meteor. Soc., 107–121, No. 24.

Bringi, V., T. Tang, and V. Chandraesekar, 2004: Evaluation of a new polarimetrically-based Z-R relation. *J. Atmos. and Ocean. Technol.*, **21**, 612–622.

Bringi, V. N., G.-J. Huang, V. Chandraesekar, and T. D. Keenan, 2001: An areal rainfall estimator using differential propagation phase: Evaluation using a C-Band radar and a dense gauge network in the tropics. *J. Atmos. and Ocean. Technol.*, **18**, 1810–1818.

Carbone, R. E., T. D. Keenan, J. Wilson, and J. M. Hacker, 2000: Tropical island convection in the absence of significant topography, Part I: Lifecycle of diurnally forced convection. *Mon. Wea. Rev.*, **128**, 3459–3480.

Chen, S.-H. and W.-Y. Sun, 2002: A one-dimensional time dependent cloud model. *J. Meteor. Soc. Japan*, **80**, 99–118.

Crook, A., 2001: Understanding Hector: The dynamics of island thunderstorms. *Mon. Wea. Rev.*, **129**, 1550–1563.

DelGenio, A. D. and W. Kovari, 2002: Climatic properties of tropical precipitating convection under varying environmental conditions. *J. Climate*, **15**, 2597–2615.

Done, J., C. A. Davis, and M. Weisman, 2004: The next generation of NWP: explicit forecasts of convection using the weather research and forecasting (WRF) model. *Atmos. Sci. Lett.*, **5**, 110–117.

Drosdowsky, W., 1996: Variability of the Australian summer monsoon at Darwin: 1957-1992. *J. Climate*, **9**, 85–96.

Dudhia, J., 1989: Numerical study of convection observed during the winter monsoon experiment using a mesoscale two-dimensional model. *J. Atmos. Sci.*, **46**, 3077–3107.

Golding, B. W., 1993: A numerical investigation of tropical island thunderstorms. *Mon. Wea. Rev.*, **121**, 1417–1433.

Grell, G. A. and D. Dévényi, 2002: A generalized approach to parameterizing convection combining ensemble and data assimilation techniques. *Geophys. Res. Lett.*, **29 (14)**, 1693–1696.

Gunn, B. W., J. L. McBride, G. J. Holland, T. D. Keenan, and N. E. Davidson, 1989: The Australian Summer Monsoon Circulation during AMEX Phase II. *Mon. Wea. Rev.*, **117**, 2554–2574.

Hamilton, K., R. A. Vincent, and P. T. May, 2004: Darwin Area Wave Experiment (DAWEX) field campaign to study gravity wave generation and propagation. *J. Geophys. Res.*, **109**, 1–15.

Holland, G. J., J. L. McBride, R. K. Smith, D. Jasper, and T. D. Keenan, 1986: The BMRC Australian Monsoon Experiment. *Bull. Amer. Meteor. Soc.*, **67**, 1466–1472.

Hong, S. Y. and J. Dudhia, 2003: Testing of a new non-local boundary layer vertical diffusion scheme in numerical weather prediction applications. *Proceedings of the 16th Conference on Numerical Weather Prediction*, Seattle, WA, Amer. Meteor. Soc.

Jakob, C., R. Pincus, C. Hannay, and K.-M. Xu, 2004: Use of cloud radar observations for model evaluation: A probabilistic approach. *J. Geophys. Res.*, doi:10.1029/2003JD003473.

Janjić, Z. I., 1994: The step-mountain eta coordinate model: Further developments of the convection, viscous sublayer, and turbulence closure schemes. *Mon. Wea. Rev.*, **122**, 927–945.

Janjic, Z. I., 2002: Nonsingular implementation of the Mellor-Yamada level 2.5 scheme in the NCEP meso model. Tech. Rep. 437, NCEP Office Note, [Available from NCEP, 5200 Auth Rd., Camp Springs, MD 20746.].

Kain, J. S., 2004: The Kain Fritsch convective parameterization: An update. *J. Appl. Meteor.*, **43**, 170–181.

Kain, J. S. and J. M. Fritsch, 1990: A one-dimensional entraining/detraining plume model and its application in convective parameterization. *J. Atmos. Sci.*, **47**, 2784–2802.

———, 1993: Convective parameterization for mesoscale models: The Kain-Fritsch scheme. *The representation of cumulus convection in numerical models*, Amer. Meteor. Soc., 165–170, No. 24.

Kain, J. S., S. J. Weiss, J. J. Levit, M. E. Baldwin, and D. R. Bright, 2006: Examination of convection-allowing configurations of the WRF model for the prediction of severe convective weather: The SPC/NSSL spring program 2004. *Wea. Forecasting*, **21**, 167–181.

Keenan, T., S. Rutledge, R. Carbone, J. Wilson, T. Takahashi, P. May, N. Tapper, M. Platt, J. Hacker, S. Sekelsky, M. Moncrieff, K. Saito, G. Holland, A. Crook, and K. Gage, 2000: The Maritime Continent Thunderstorm Experiment (MCTEX): Overview and Some Results. *Bull. Amer. Meteor. Soc.*, **81**, 2433–2455.

Keenan, T. D. and R. E. Carbone, 1992: A preliminary morphology of precipitation systems in tropical northern Australia. *Quart. J. Roy. Meteor. Soc.*, **118**, 283–326.

Keenan, T. D., K. Glasson, F. Cummings, T. S. Bird, J. Keeler, and J. Lutz, 1998: The BMRC/NCAR C-Band polarimetric (C-POL) radar system. *J. Atmos. and Ocean. Technol.*, **15**, 871–886.

Keenan, T. D., B. R. Morton, M. J. Manton, and G. J. Holland, 1989: The Island Thunderstorm Experiment (ITEX) - a study of tropical thunderstorms in the maritime continent. *Bull. Amer. Meteor. Soc.*, **70**, 152–159.

Lane, T. P. and M. J. Reeder, 2001: Modelling the generatin of gravity waves by a maritime continent thunderstorm. *Quart. J. Roy. Meteor. Soc.*, **127**, 2705–2724.

Lo, J. C., Z. Yang, and R. A. Pielke, 2008: Assessment of three dynamical climate downscaling methods using the Weather Research and Forecasting (WRF) model. *J. Geophys. Res.*, **113**, doi:10.1029/2007JD009216.

May, P. T. and A. Ballinger, 2007: The statistical characteristics of convective cells in a monsoon regime (Darwin, northern Australia). *Mon. Wea. Rev.*, **135**, 8292.

May, P. T., J. H. Mather, G. Vaughan, C. Jakob, G. M. McFarquar, K. N. Bower, and G. G. Mace, 2008: The Tropical Warm Pool International Cloud Experiment (TWP-ICE). *Bull. Amer. Meteor. Soc.*, doi:10.1175/BAMS-89-2-153.

Mlawer, E. J., S. J. Taubman, P. D. Brown, M. J. Iacono, and S. A. Clough, 1997: Radiative transfer for inhomogeneous atmosphere: RRTM, a validated correlated-k model for the long-wave. *J. Geophys. Res.*, **102 (D14)**, 16 663–16 682.

Neale, R. and J. Slingo, 2003: The maritime continent and its role in the global climate: a GCM study. *J. Climate*, **16**, 834–848.

Pautet, P.-D., M. J. Taylor, A. . Liu, and G. R. Swenson, 2005: Climatology of short-period gravity waves observed over northern Australia during the Darwin Area Wave Experiment (DAWEX) and their dominant source regions. *J. Geophys. Res.*, **110**, 1–13.

Skamarock, W. C., J. B. Klemp, J. Dudhia, D. O. Gill, D. M. Barker, W. Wang, and J. G. Powers, 2002: A description of the advanced research WRF version 2. Tech. Rep. NCAR/TN-468+STR, NCAR Tech Note, [Available from UCAR Communications, P.O. Box 3000, Boulder, CO 80307].

Stoelinga, M. T., 2005: Simulated equivalent reflectivity factor as currently formulated in RIP: Description and possible improvements. Tech. rep., Unpublished manuscript, [Available from www.atmos.washington.edu/ stoeling/RIP_sim.pdf].

Wang, Y., L. Zhou, and K. P. Hamilton, 2007: Effect of convective entrainment/detrainment on simulation of tropical precipitation diurnal cycle. *Mon. Wea. Rev.*, **135**, 567–585.

Wapler, K., T. Lane, P. May, C. Jakob, S. Siems, and M. Manton, 2008: WRF model simulations of tropical cloud systems observed during TWP-ICE. *Extended Abstracts, 28th Conference on Hurricanes and Tropical Meteorology*, Orlando, FL, Amer. Meteor. Soc.

Warner, T. T. and H.-M. Hsu, 2000: Nested-model simulation of moist convection: the impact of coarse-grid parameterized convection on fine-grid resolved convection. *Mon. Wea. Rev.*, **128**, 2211–2231.

Weisman, M. L., C. Davis, W. Wang, K. W. Manning, and J. B. Klemp, 2008: Experimences with 0-36-h explicit convective forecasts with the WRF-ARW model. *Wea. Forecasting*, **23**, 407–437.

Yang, G.-Y. and J. Slingo, 2001: The diurnal cycle in the tropics. *Mon. Wea. Rev.*, **129**, 784–801.

Zhang, M. H., J. L. Lin, R. T. Cederwall, J. J. Yio, and S. C. Xie, 2001: Objective analysis of ARM IOP data: Method and sensitivity. *Mon. Wea. Rev.*, **129**, 295–311.

List of Figures

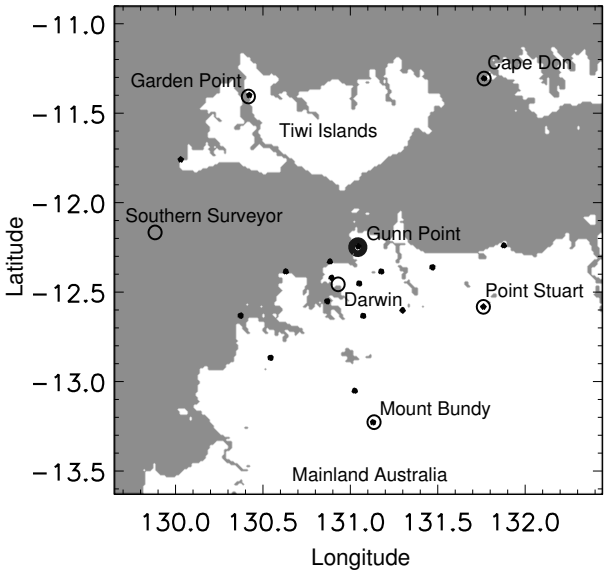

FIG. 1. Map of area of interest including the location of radar (thick dot), rain gauges (thin dots) and radiosonde sites (circles).

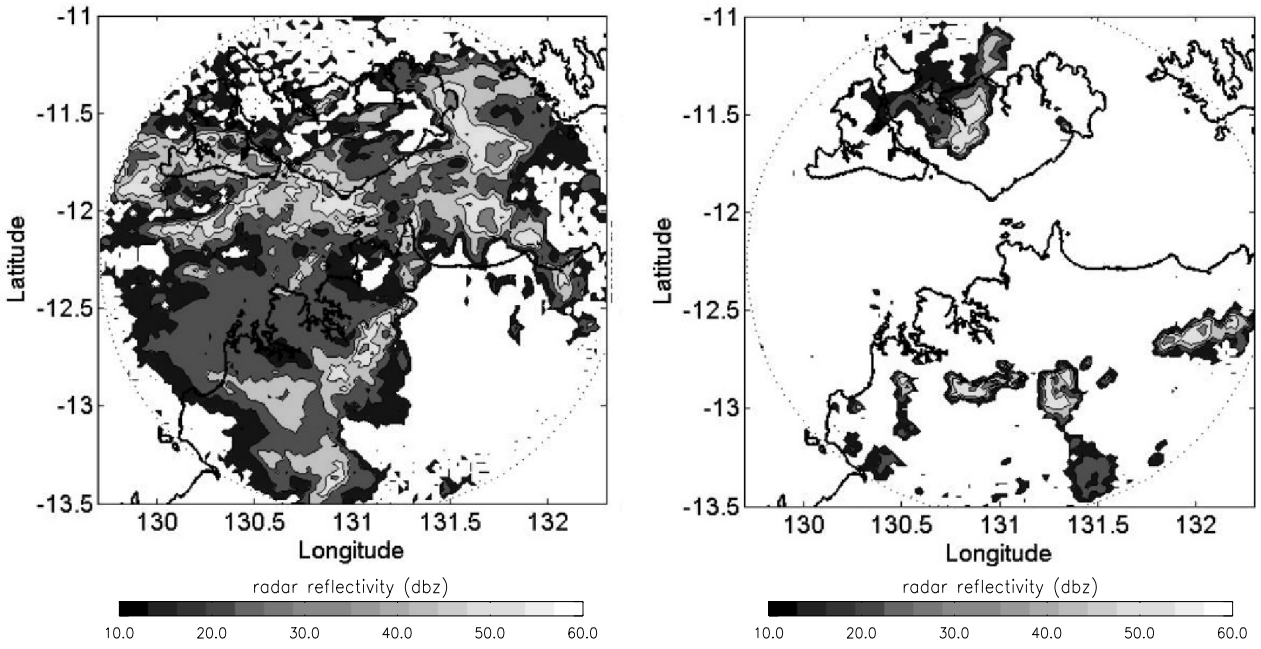

FIG. 2. Example of reflectivities measured with radar for (a) the active monsoon (0030 LT 24 January 2007) and (b) the break period (1800 LT 06 February 2007). Contours are drawn every 10 dBZ from 10 dBZ.

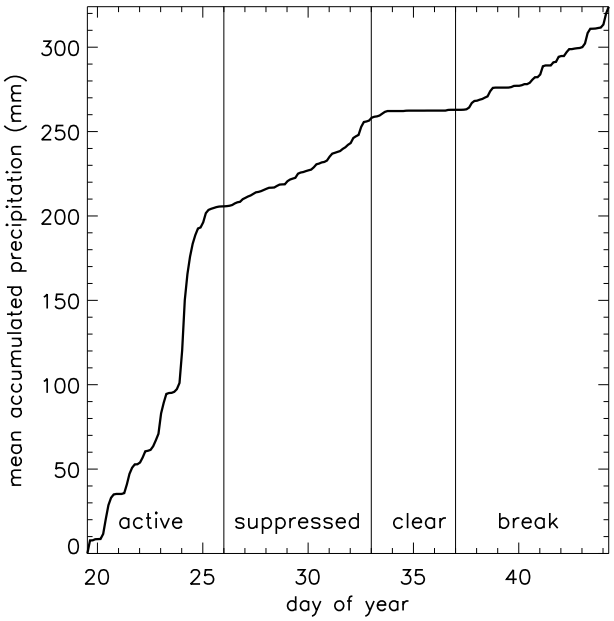

FIG. 3. Area averaged accumulated precipitation during TWP-ICE derived from radar observations, along with classification of the four observed regimes. The precipitation was averaged over the area covered by the radar range.

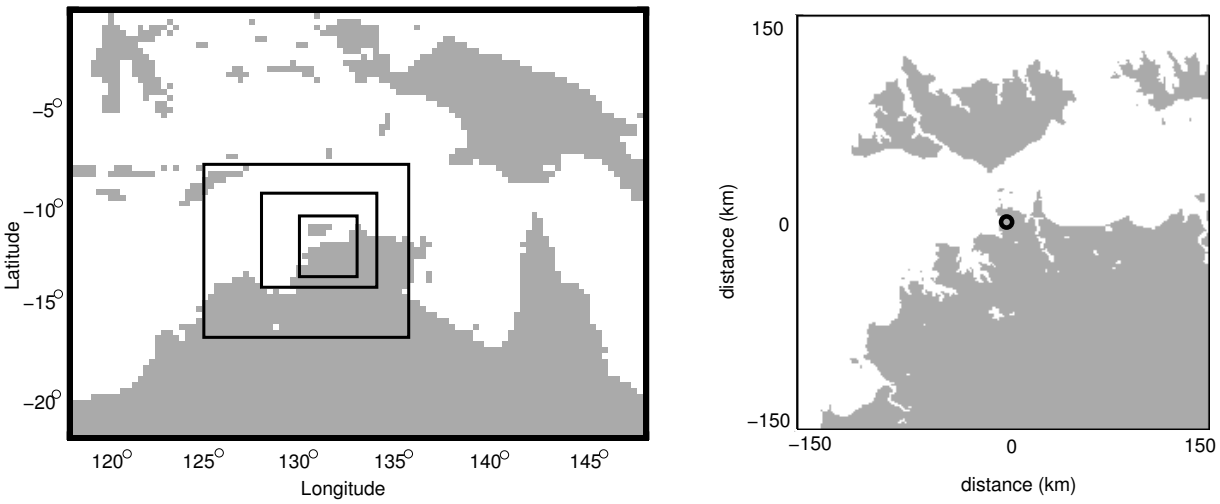

FIG. 4. Outer simulation domain (left), along with the three nested inner domains. The inner domain (right) showing the location of the radar.

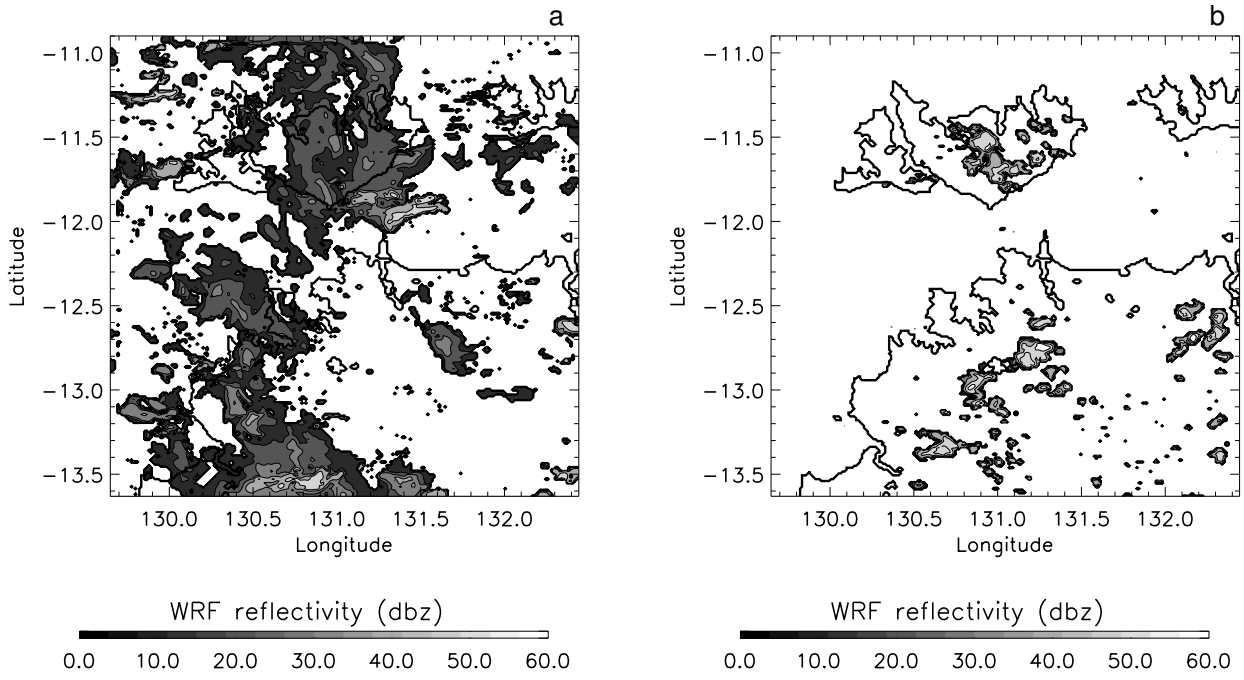

FIG. 5. Example of the column maximum reflectivities calculated from WRF simulations for (a) the active monsoon (2230 LT 23 January 2006) and (b) the monsoon break period (1630 LT 06 February 2006).

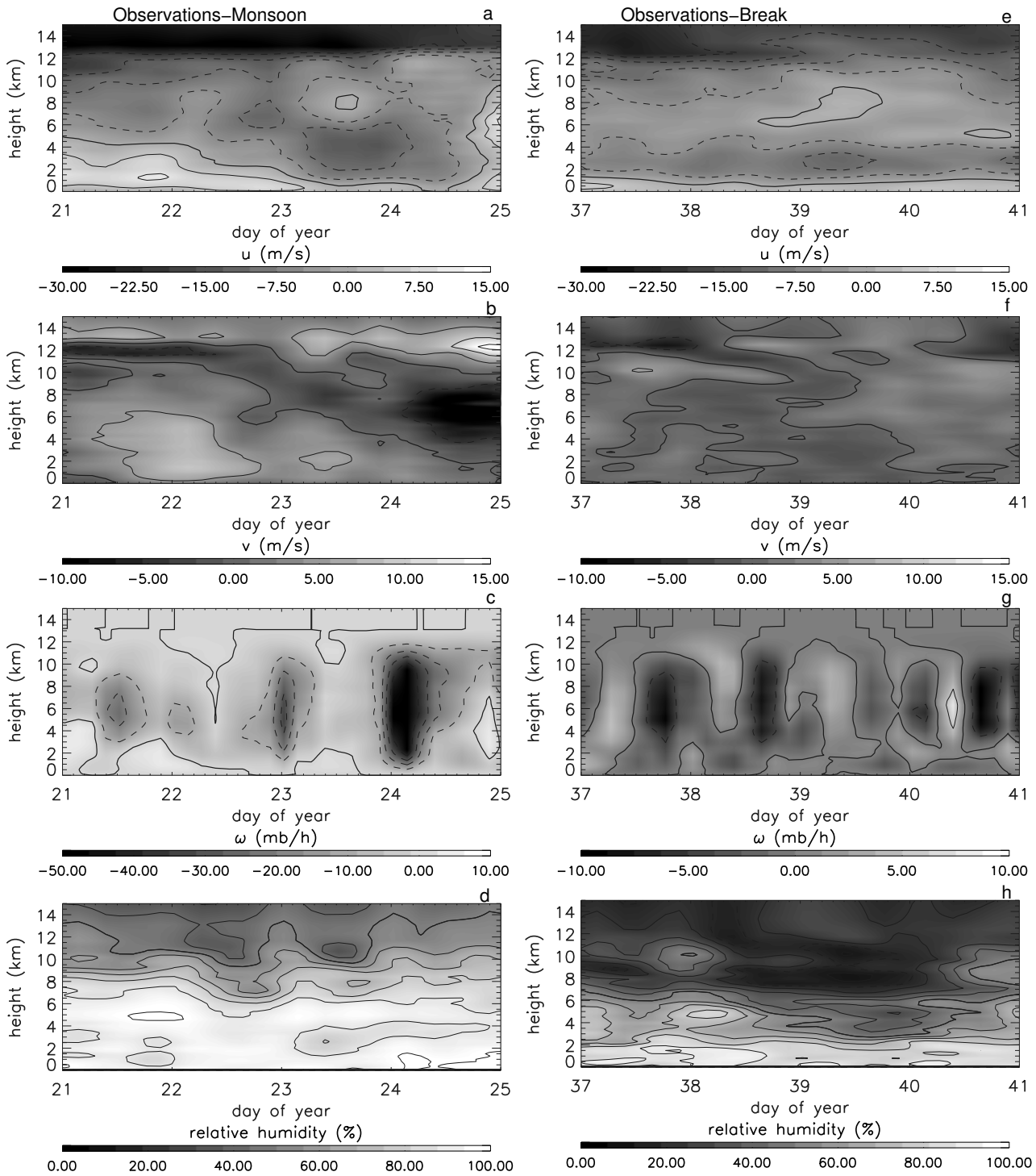

FIG. 6. Time height cross-section of observed averaged (a-b, e-f) horizontal velocity, (c, g) omega and (d, h) relative humidity with respect to water for (a-d) the active monsoon and (e-h) the break period. Contour lines are drawn at intervals of 5 m/s, 10 mb/h and 10%. In a-c, e-g the thick contour denotes zero, and negative values are dashed. In d, h the thick contour denotes 50%. Times are local.

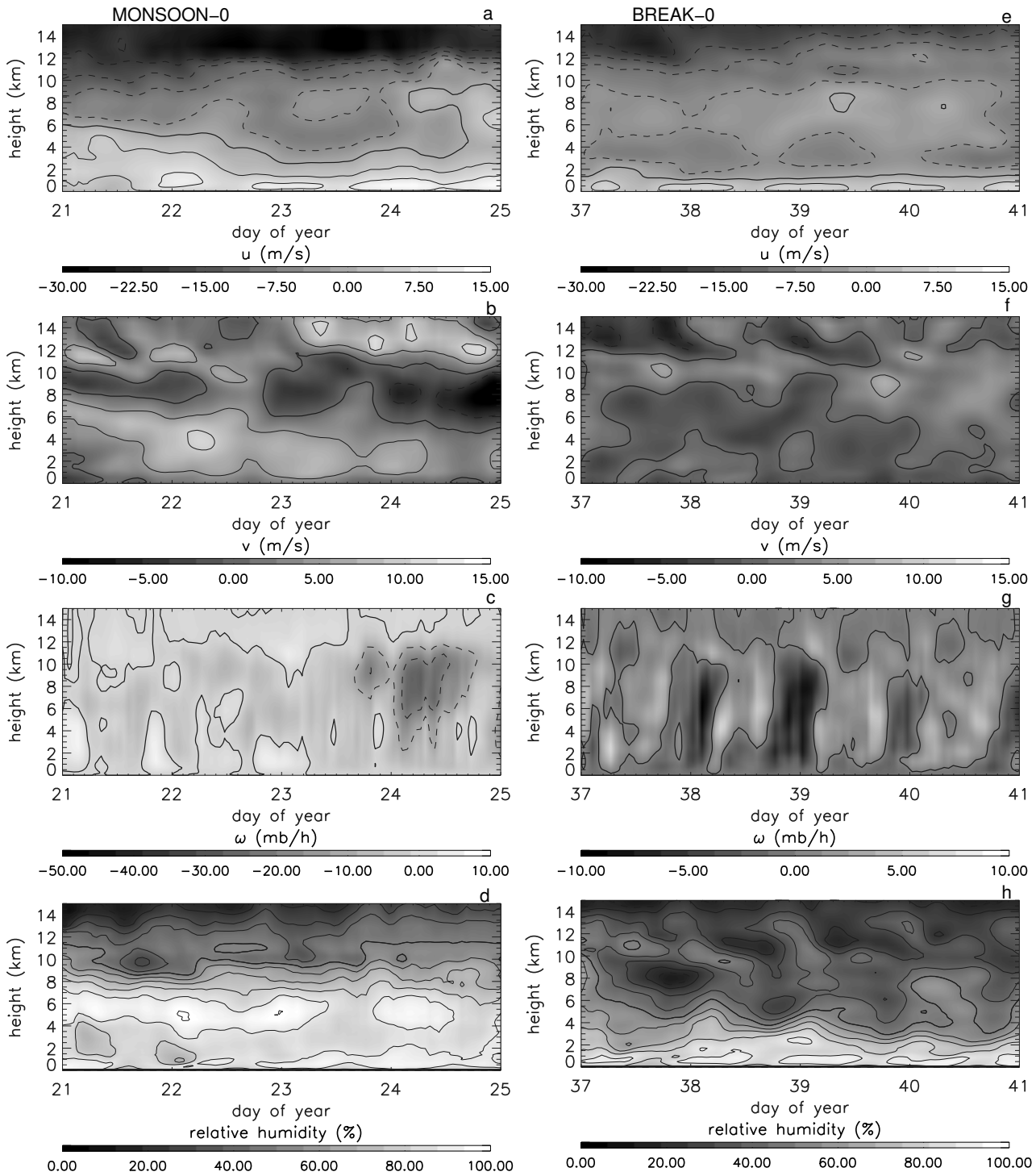

FIG. 7. Time height cross-section of simulated averaged (a-b, e-f) horizontal velocity, (c, g) omega and (d, h) relative humidity with respect to water for (a-d) the active monsoon (MONSOON-0) and (e-h) the break period (BREAK-0). Contour lines are drawn at intervals of 5 m/s, 10 mb/h and 10%. In a-c, e-g the thick contour denotes zero, and negative values are dashed. In d, h the thick contour denotes 50%. Times are local.

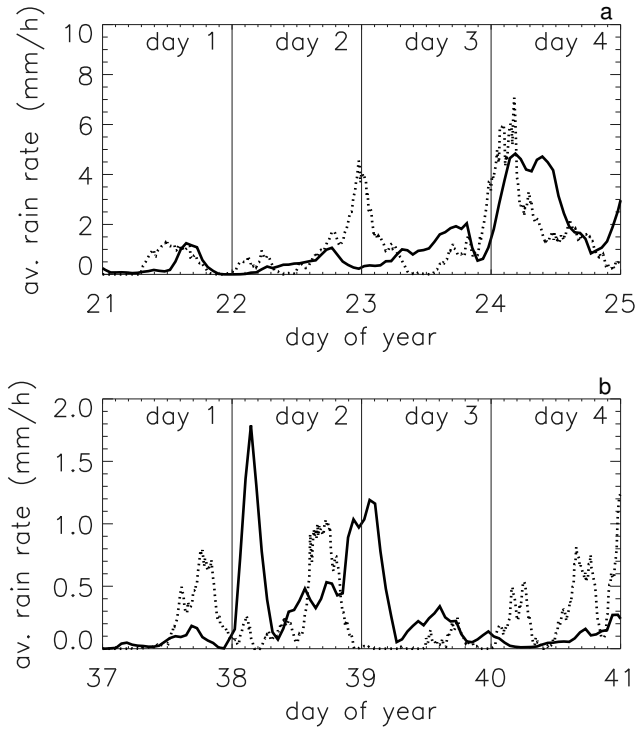

FIG. 8. Area averaged rain rates from the polarimetric radar (dotted) and WRF simulations (solid), for (a) the active monsoon (MONSOON-0) and (b) the break period (BREAK-0).

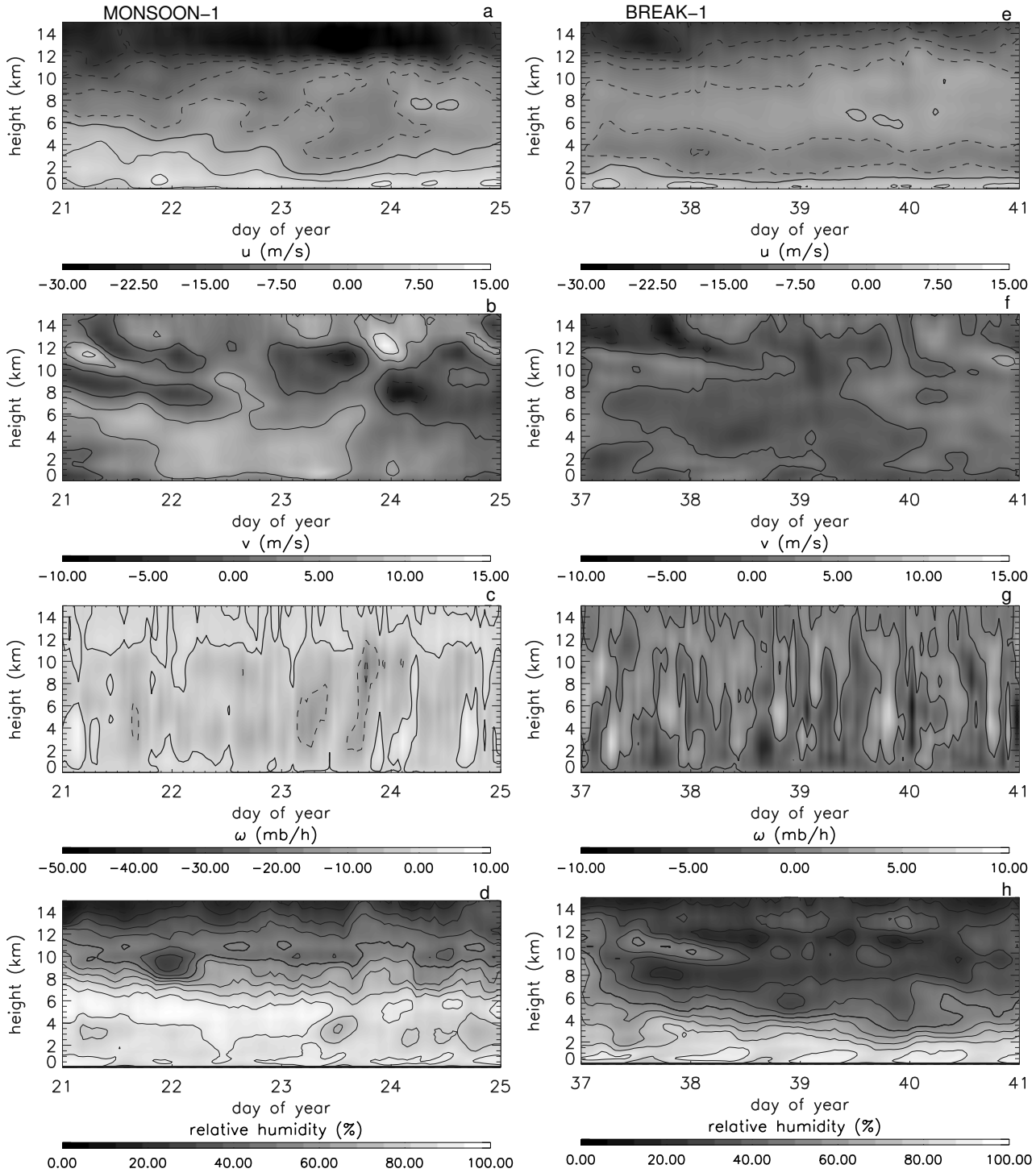

FIG. 9. Time height cross-section of simulated averaged (a-b, e-f) horizontal velocity, (c, g) omega and (d, h) relative humidity with respect to water for (a-d) the active monsoon (MONSOON-1) and (e-h) the break period (BREAK-1). Contour lines are drawn at intervals of 5 m/s, 10 mb/h and 10%. In a-c, e-g the thick contour denotes zero, and negative values are dashed. In d, h the thick contour denotes 50%. Times are local.

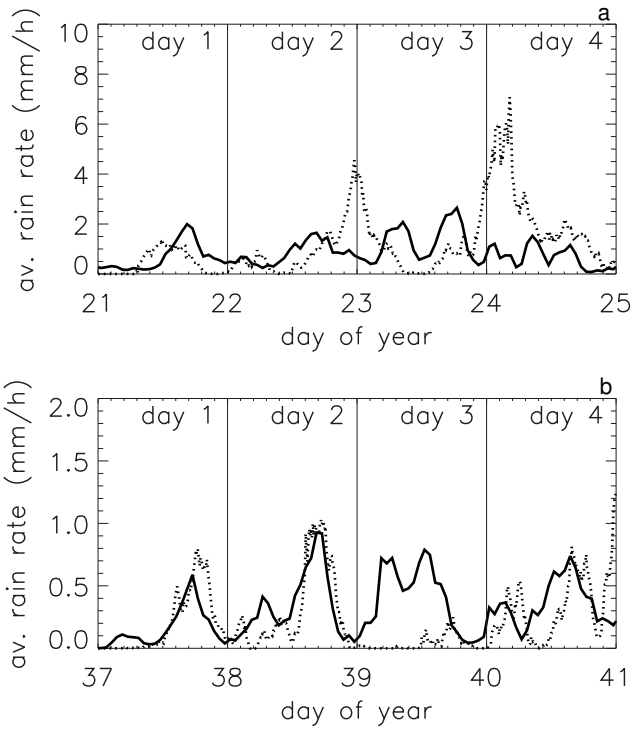

FIG. 10. Area averaged rain rates from the polarimetric radar (dotted) and WRF simulations (solid), for (a) the active monsoon and (b) the break period; results from the simulations MONSOON-1 and BREAK-1 (without cumulus parametrization).

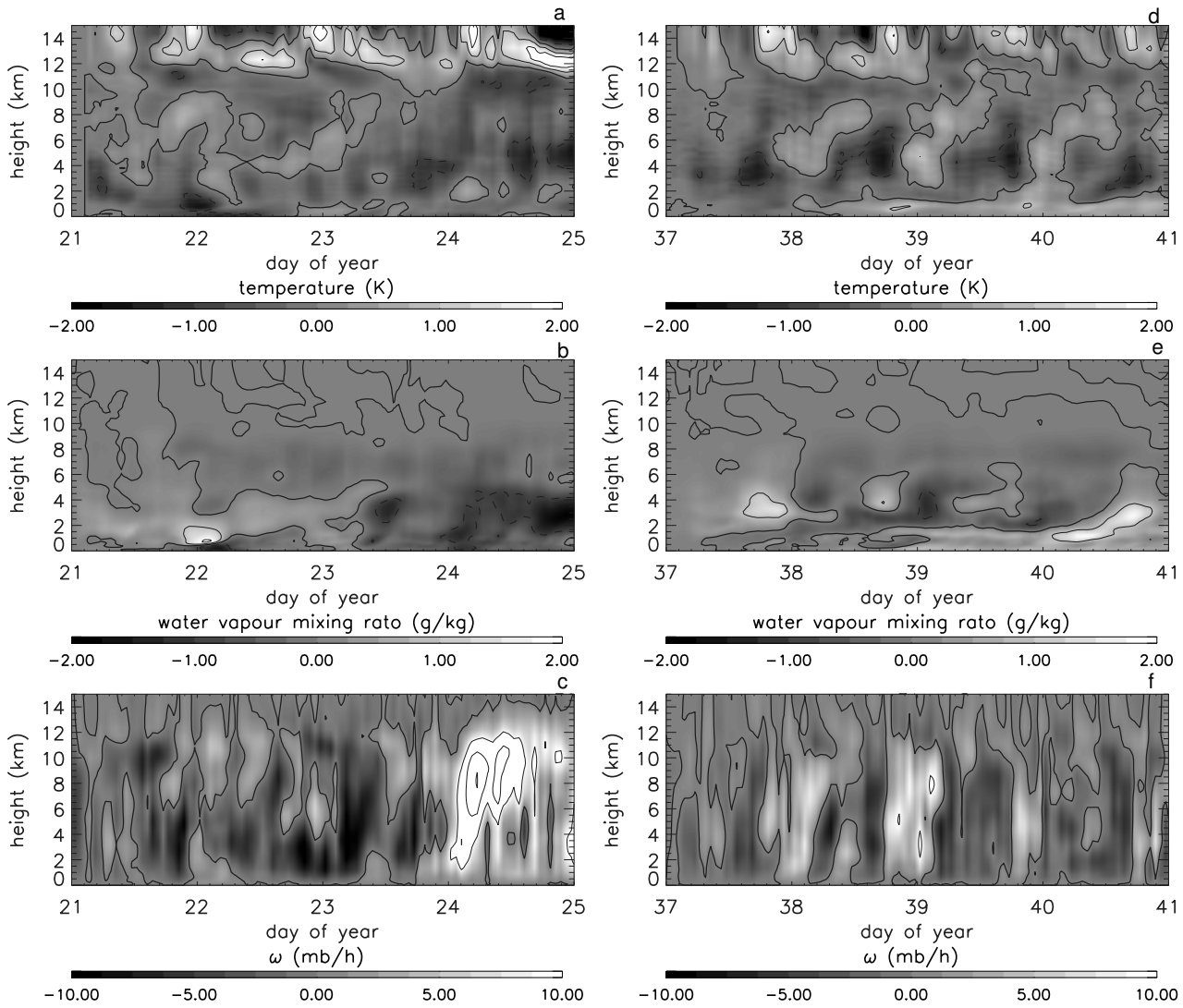

FIG. 11. Time height cross-section of difference between mean profiles from (a-c) the MONSOON-1 minus the MONSOON-0 simulation and (d-f) the BREAK-1 minus BREAK-0 simulation: (a, d) temperature, (b, e) water vapour mixing ratio and (c, f) omega. Contour lines are drawn at intervals of 1 K, 1 g/kg and 10 mb/h.

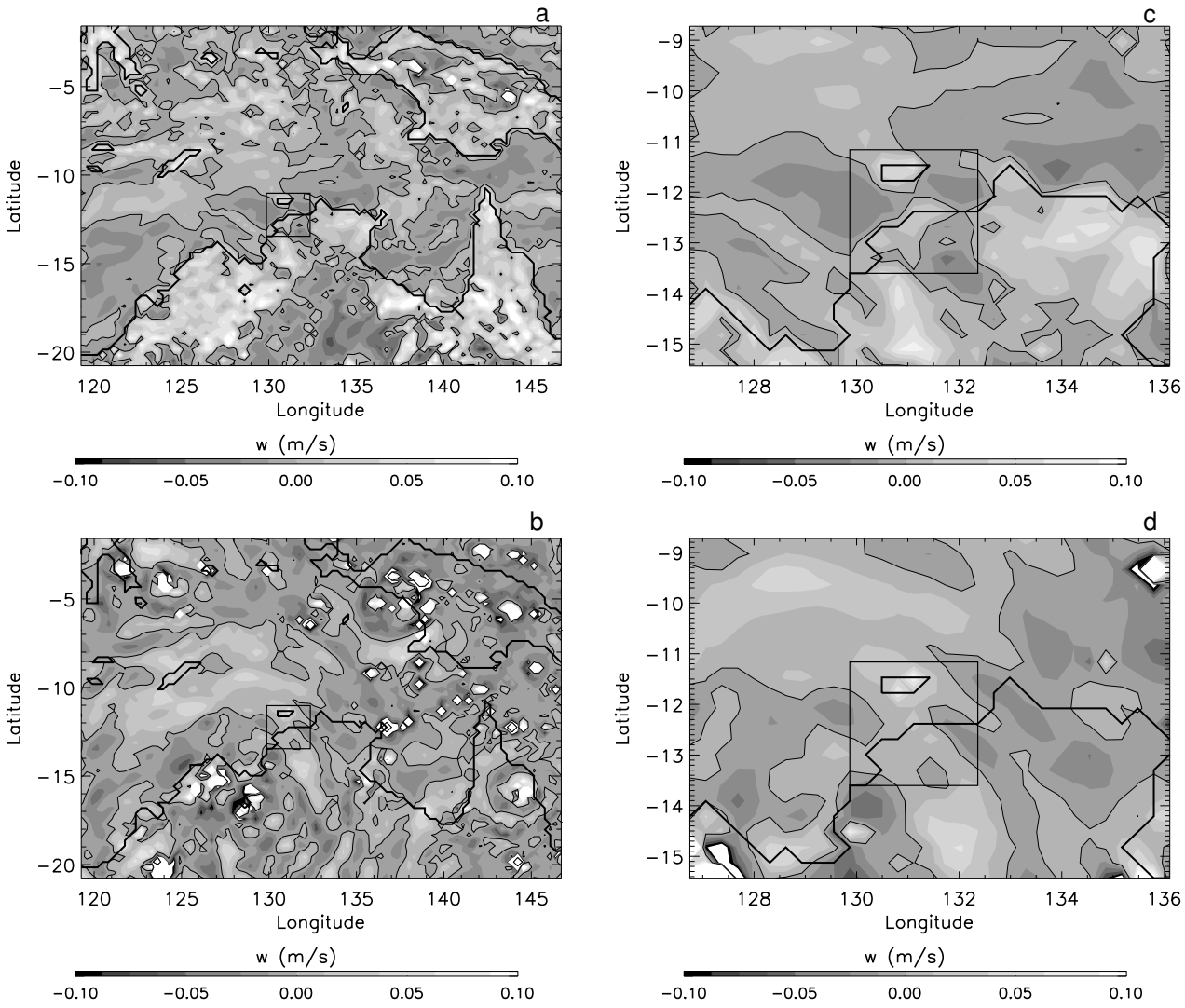

FIG. 12. Vertical velocity at 3 km at 1330 LT 6 February 2006 from (a, c) the reference simulation BREAK-0 and (b, d) the simulation without cumulus parametrization (BREAK-1); results from the coarsest grid (a-b) in the whole domain and (c-d) in the area of interest.

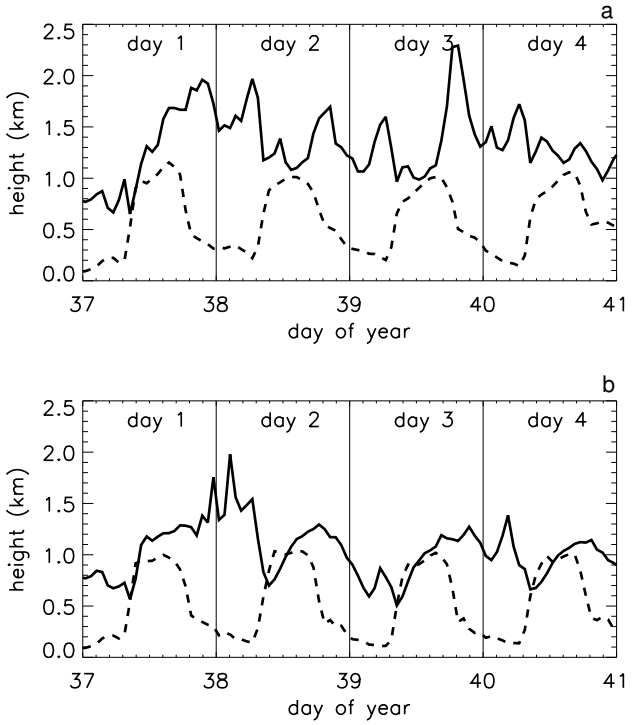

FIG. 13. Mean level of free convection (solid) and boundary layer height (dashed) over land of the inner-most domain from (a) the reference simulation BREAK-0 and (b) the simulation without cumulus parametrization (BREAK-1).

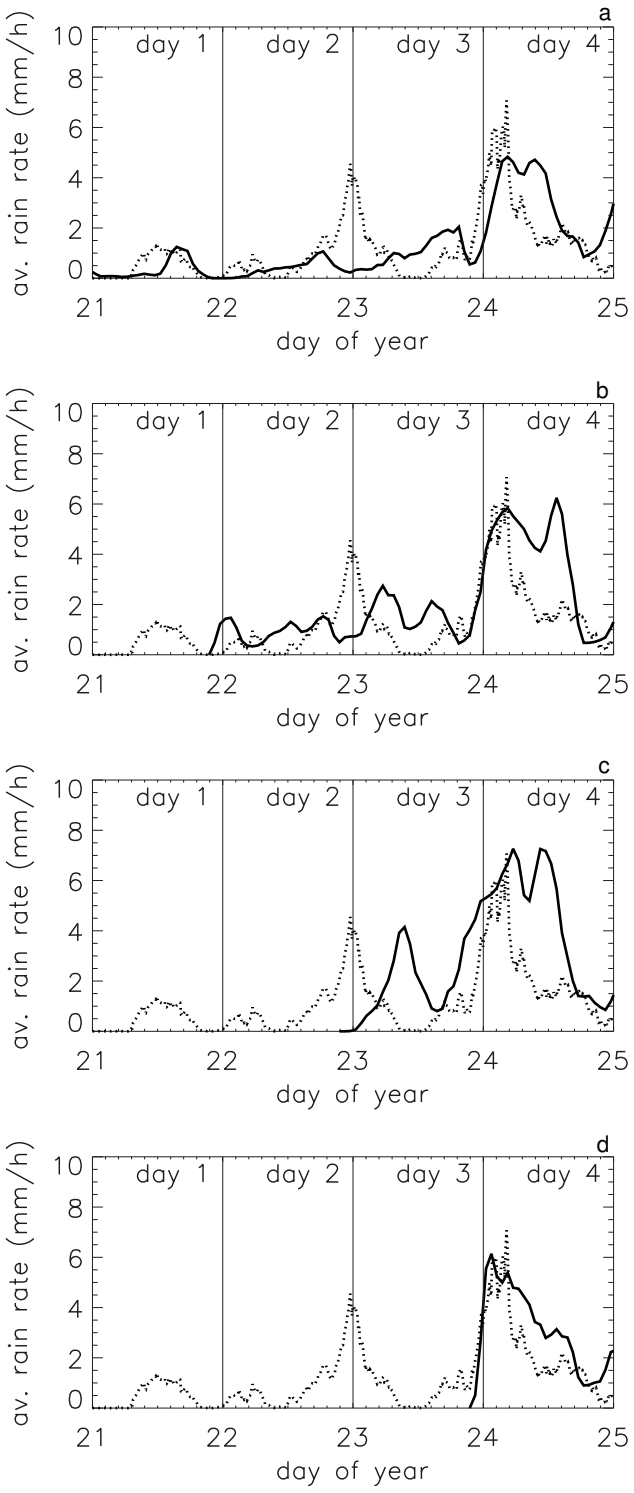

FIG. 14. Area averaged rain rates from the polarimetric radar (dotted) and WRF simulations (solid) for the active monsoon, results from the simulation initialized at (a) 1200 UTC 20 January 2006 (MONSOON-0), (b) at 1200 UTC 21 January 2006 (MONSOON-2), (c) at 1200 UTC 22 January 2006 (MONSOON-3) and (d) at 1200 UTC 23 January 2006 (MONSOON-4).

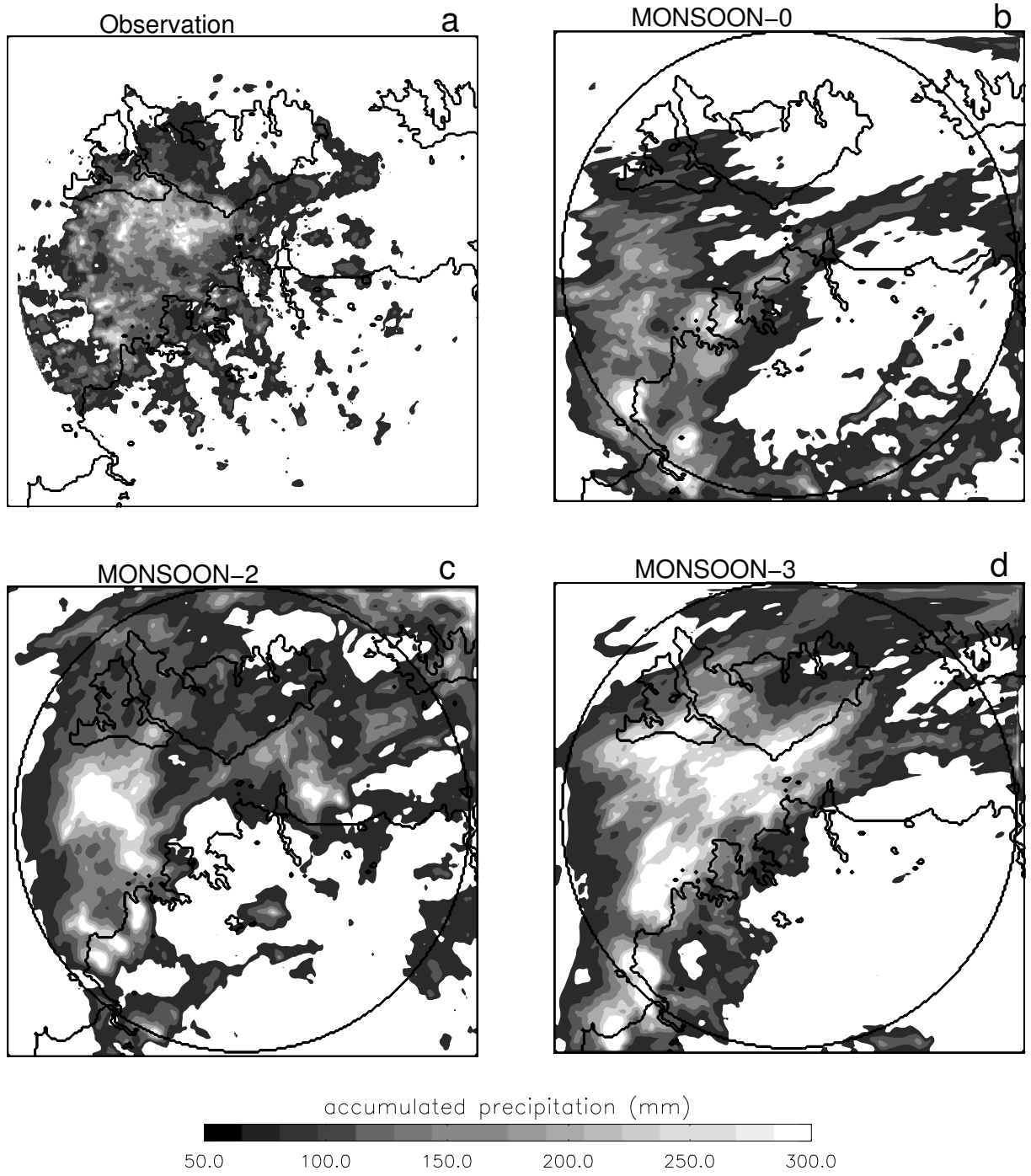

FIG. 15. Map of accumulated precipitation on day 4 from (a) radar, (b) MONSOON-0, (c) MONSOON-2, and (d) MONSOON-3 simulation. Contours are drawn every 50 mm, starting at 50 mm. The circle shows the range of radar observations, it has a radius of 150 km and is centered at Gunn Point (12.25°S, 131.04°E).

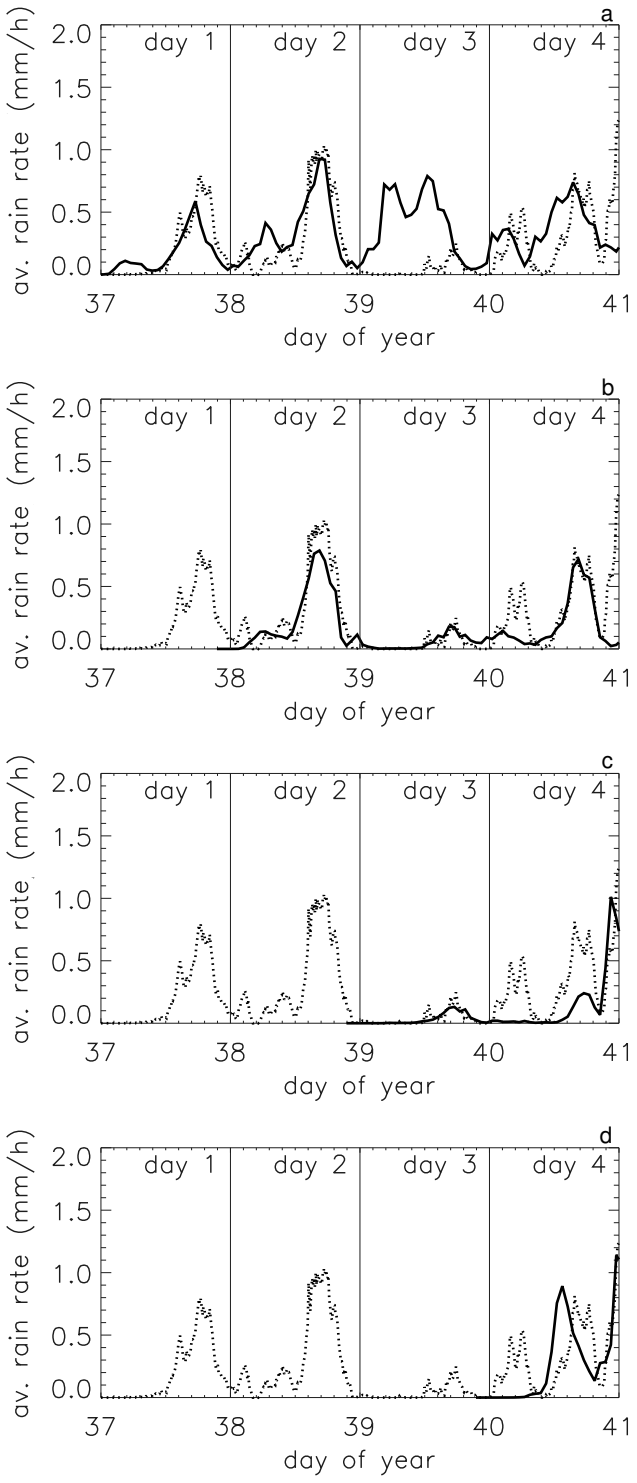

FIG. 16. Area averaged rain rates from the polarimetric radar (dotted) and WRF simulations (solid) for the break period, results from the simulation initialized at (a) 1200 UTC 5 February 2006 (BREAK-1), (b) at 1200 UTC 6 February 2006 (BREAK-2), (c) at 1200 UTC 7 February 2006 (BREAK-3), and (d) at 1200 UTC 8 February 2006 (BREAK-4).

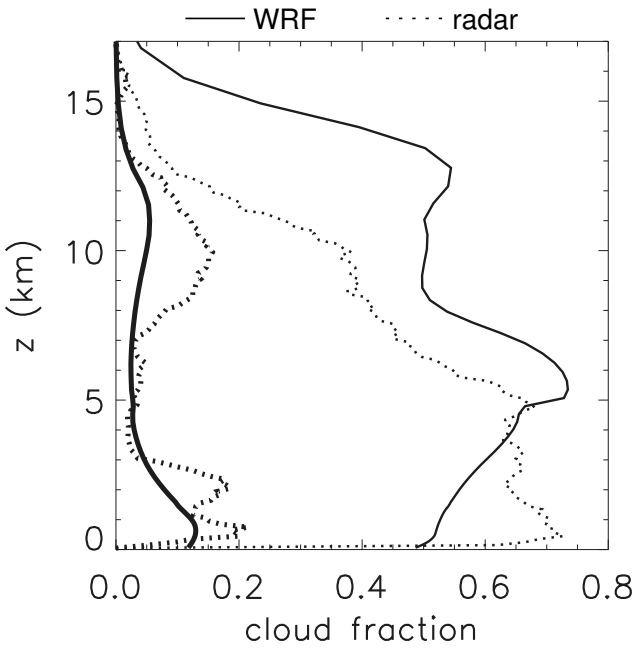

FIG. 17. Mean cloud fraction profiles for active monsoon (thin, MONSOON-0) and break (thick, BREAK-1) from WRF (solid) and the cloud frequency from the radar observations (dotted).

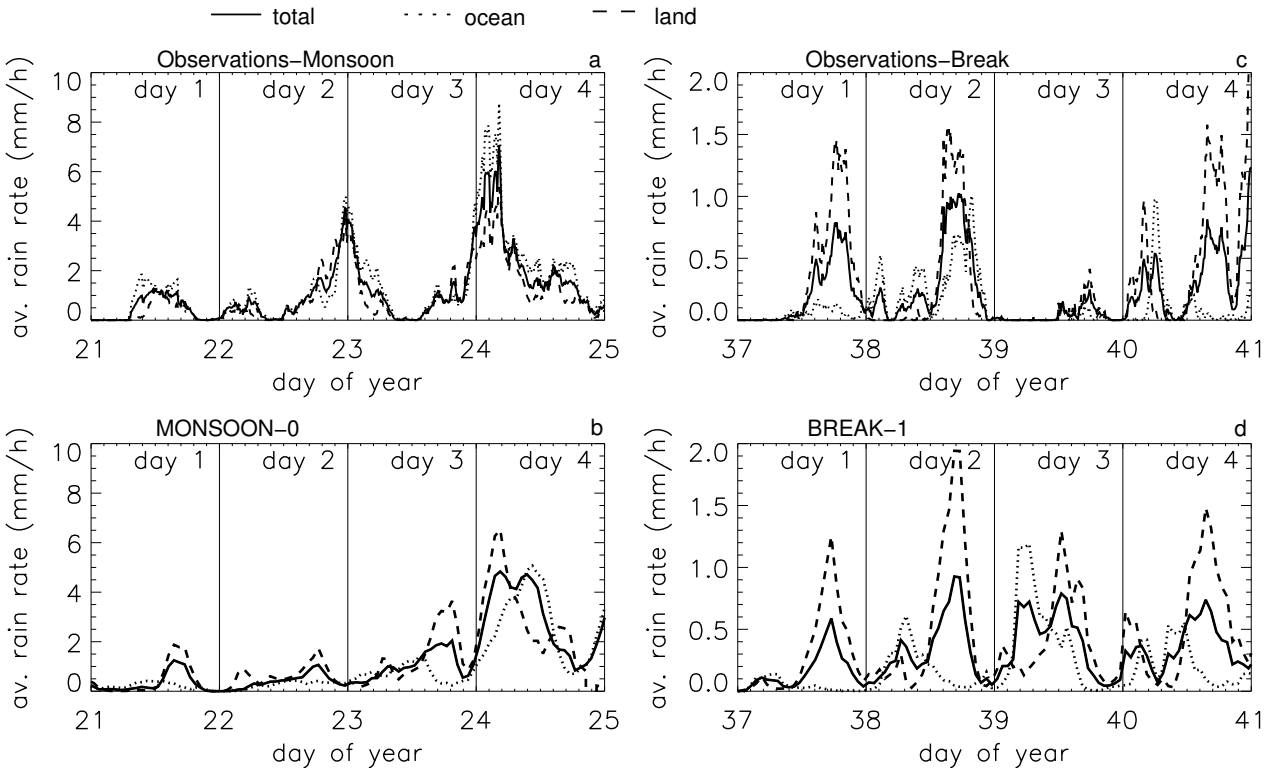

FIG. 18. Area averaged rain rates from (a, c) the polarimetric radar and (b, d) WRF simulations separated between land (dashed), ocean (dotted) and total (solid) for (a-b) the monsoon and (c-d) the break period; results from the simulation MONSOON-0 and BREAK-1.

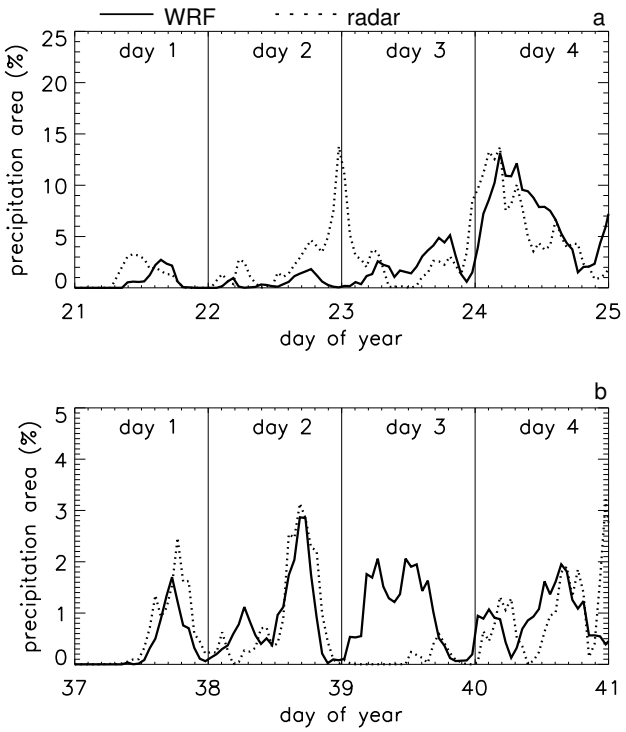

FIG. 19. Areas covered by rain rates of at least 10mm/h from the polarimetric radar (dotted) and WRF simulations (solid) for (a) the monsoon and (b) the break period; results from the simulations MONSOON-0 and BREAK-1.

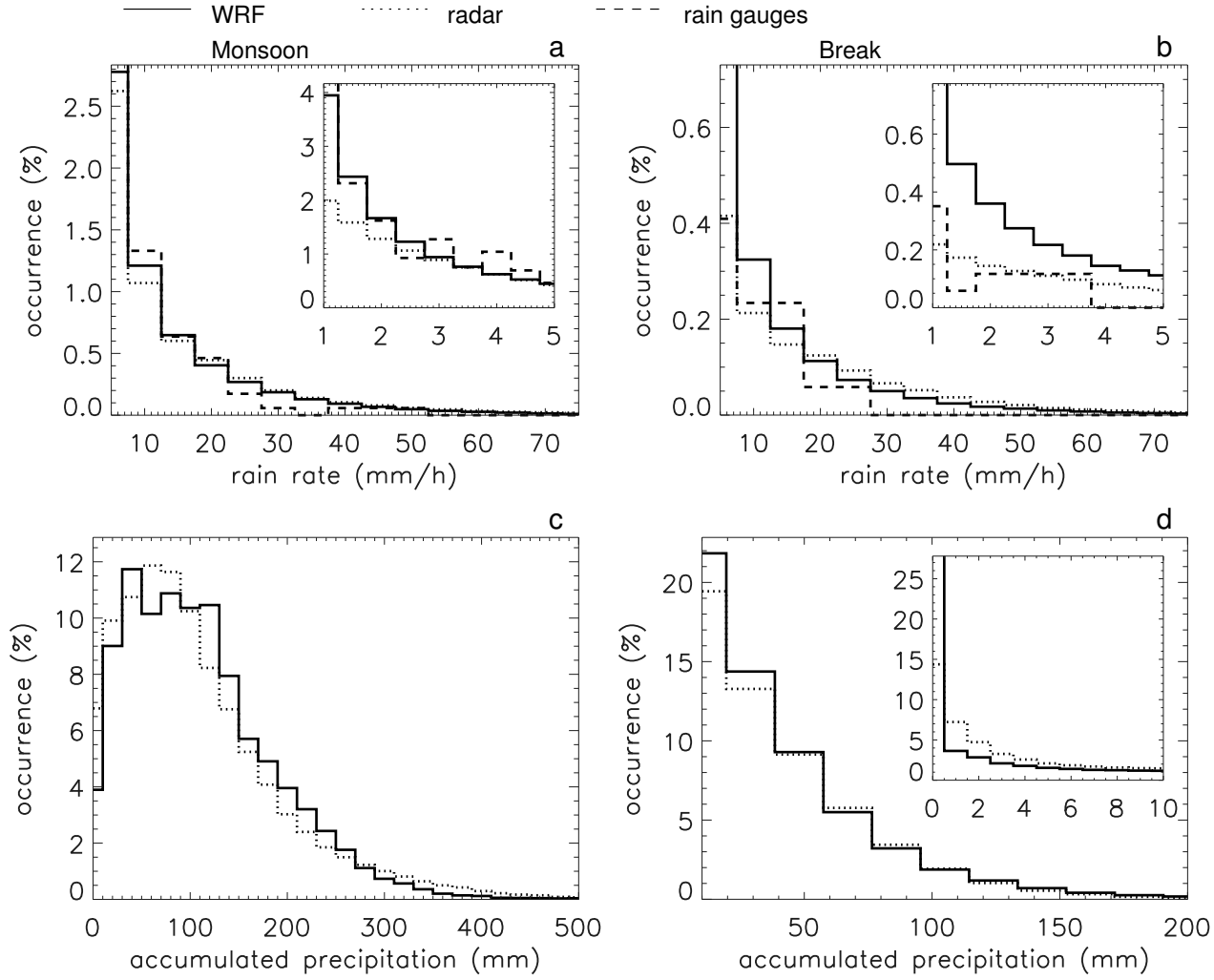

FIG. 20. Histogram of rain rates from the polarimetric radar (dotted), rain gauges (dashed) and WRF simulations (solid), for (a) the active monsoon (MONSOON-0) and (b) the break period (BREAK-1) and histogram of accumulated rain during the simulated 4-day period of (c) the active monsoon and (d) the break period from the polarimetric radar (dotted) and WRF simulations (solid). Nested plots in (a-b) and (d) show histograms for low rain rates and low accumulated precipitation.

List of Tables

TABLE 1. Overview of WRF configuration.

domain	horizontal resolution (km)	grid size	location of SW corner	cumulus parameterization
1	34	100×75	22.22°S, 117.70°E	yes
2	11.333	100×85	16.73°S, 125.09°E	yes
3	3.778	160×136	14.36°S, 127.86°E	no
4	1.259	244×244	13.63°S, 129.65°E	no

TABLE 2. Overview of WRF simulations for monsoon and break period (KF: Kain-Fritsch scheme).

name	initialization	cumulus scheme
MONSOON-0	2006/01/20 1200	KF
MONSOON-1	2006/01/20 1200	no
MONSOON-2	2006/01/21 1200	KF
MONSOON-3	2006/01/22 1200	KF
MONSOON-4	2006/01/23 1200	KF
BREAK-0	2006/02/05 1200	KF
BREAK-1	2006/02/05 1200	no
BREAK-2	2006/02/06 1200	no
BREAK-3	2006/02/07 1200	no
BREAK-4	2006/02/08 1200	no